Atmos. Chem. Phys. Discuss., 9, 8993–9042, 2009
www.atmos-chem-phys-discuss.net/9/8993/2009/

Atmospheric Chemistry and Physics Discussions

This discussion paper is/has been under review for the journal *Atmospheric Chemistry and Physics (ACP)*. Please refer to the corresponding final paper in *ACP* if available.

Temporal and spatial variability of glyoxal as observed from space

M. Vrekoussis, F. Wittrock, A. Richter, and P. J. Burrows

Institute of Environmental Physics and Remote Sensing, IUP, University of Bremen, NW1, P.O. Box 330440, 28334, Bremen, Germany

Received: 16 March 2009 – Accepted: 16 March 2009 – Published: 3 April 2009

Correspondence to: M. Vrekoussis (vrekoussis@iup.physik.uni-bremen.de)

Published by Copernicus Publications on behalf of the European Geosciences Union.

Abstract

Glyoxal, CHO.CHO, is produced during the oxidation of volatile organic compounds, VOC, released by anthropogenic activities, biogenic processes and biomass burning. It has a short chemical lifetime of a few hours in the boundary layer and lower troposphere and therefore serves as an indicator and a marker of photochemical hot-spots and their response to changing atmospheric conditions around the globe. For this reason more than five years of CHO.CHO observations (2002–2007), retrieved from the radiances measured by the satellite instrument SCIAMACHY, were obtained and analyzed both temporally and spatially. The largest columns of CHO.CHO ($>6\times10^{14}$ molec cm^{-2}) are found in the tropical and sub-tropical regions, associated with high biological activity and the plumes from vegetation fires. The majority of the identified hot spots are characterized by a well-defined seasonality: the highest values being observed during the warm and dry periods as a result of the enhanced isoprene emissions and/or biomass burning from natural or man-made fires. The regions influenced by anthropogenic pollution also encounter enhanced amounts of CHO.CHO. The ratio "CHO.CHO to HCHO, R_{GF}" over the biogenically influenced photochemical hot-spots is approximately 0.045. The presence of pyrogenic and anthropogenic emission seems to increase or decrease this number, respectively. Although the 2002–2007 period of observation is limited, over the northeastern Asia a significant annual increase in CHO.CHO in addition to a seasonal cycle is reported.

1 Introduction

The emission of Volatile Organic Compounds (VOCs), released by a variety of processes at the Earth's surface, supplies reactive carbon containing compounds to the Earth's atmosphere. Tens of thousands of different VOCs exist in the air and as a result of their reactivity have highly variable but small mixing ratios such as a few tenths of parts per billion (ppbv) or per trillion (pptv). Their occurrence influences significantly

ACPD

9, 8993–9042, 2009

atmospheric chemistry. VOCs are i) precursors of and provide the fuel for the formation of tropospheric ozone, O_3, (Houwelling et al., 1998; Wang et al., 1998a,b; Poisson et al., 2001), ii) determine the oxidizing capacity of the troposphere (Monks, 2005), iii) play an important role in controlling the Secondary Organic Aerosols (SOA) formation (Tsigaridis and Kanakidou, 2003, 2007; Kanakidou et al., 2005; Tsigaridis et al., 2005; Volkamer et al., 2006) and iv) impact on the cloud condensation nuclei (CCN) formation (Yu 2000; Roberts et al., 2002). The air pollution resulting from VOC chemistry has direct and indirect impacts on climate change (Ramanathan and Crutzen, 2003) and human health (Pope and Dockery, 2006). For all these reasons it is important to have an improved knowledge of the sources and the sinks of the VOCs and their oxidation.

1.1 Sources of VOCs (general)

Integrated over the globe, the emission of biogenic volatile organic compounds (BVOCs) overwhelms the release of VOC from anthropogenic sources: $1300\,\mathrm{Tg\,y^{-1}}$ of BVOCs are estimated to be emitted annually into the atmosphere in the form of species such as isoprene, terprenes and other oxygenated organic compounds from the biosphere whereas, human sources release approximately $100\,\mathrm{Tg\,y^{-1}}$ (Williams, 2004). The majority of the man-made emissions originate from incomplete fossil fuel combustion in energy production, transport and biomass burning. In addition significant release occurs from industrial facilities, solvent usage and oil refining.

Over the last decade an increasing effort has been made to identify the large number of VOC species present in the atmosphere and to quantify their emissions. The large variability of the fluxes of VOC to the atmosphere and their spatial distribution, make the assessment and quantification of their role in atmospheric chemistry and climate change challenging. As the development of robust strategies to reduce O_3 and aerosol levels requires the identification and quantification of VOCs, the observation of smaller molecules, which are produced in their oxidation and whose amount and distribution constrain the VOC fluxes to the atmosphere, offers a complementary approach to the measurement of VOC. The products of the VOC oxidation such as HCHO, CHO.CHO,

ACPD
9, 8993–9042, 2009

carbon monoxide (CO) and even the ultimate carbon product of their oxidation, carbon dioxide, CO_2, provide an opportunity to assess the total fluxes of VOC to the atmosphere. While the role of CO and HCHO in our efforts to understand the oxidation of species in the atmosphere has been given much attention, the use of CHO.CHO, for which the first measurements have only recently been reported, to constrain our understanding of the impact of VOC chemistry, remains relatively unexploited.

1.2 CHO.CHO sources

CHO.CHO is one of the most prevalent carbonyl compounds in the atmosphere. It is the smallest alpha-dicarbonyl formed by chemical reactions following the initial elementary oxidation of VOC. The information about the distribution of direct or primary and indirect or secondary sources of CHO.CHO is poor because of the scarcity of observations. Concerning primary sources Kean et al., (2001) and Grosjean et al., (2001) reported, during on-road measurements of carbonyl compounds at tunnels, that the emission factor of CHO.CHO ranges from 0.085 to 1.03 mg L^{-1} (or else 0.33 mg/km) depending on the type of vehicles. This number, coming from the tailpipe emissions, is significantly lower than the one observed for HCHO which was up to 38 mg L^{-1}, (Grosjean et al., 2001). One year later Hays et al., (2002) found that low molecular weight carbonyls such as HCHO, CHO.CHO, acetone, CH_3COCH_3, acetaldehyde, CH_3CHO and methyglyoxal, $CH_3CO.CHO$, are the most abundant emission under foliar fuel combustion. It has been observed that CHO.CHO emissions outweigh HCHO emissions by more than a factor of two.

CHO.CHO is produced in the oxidation of precursor hydrocarbons having two or more carbon atoms (Calvert et al., 2000, 2002). The initial attack in the troposphere proceeds mainly through the OH radicals but to a lesser extend through O_3 and nitrate radicals, NO_3. A large fraction of the first generation CHO.CHO production ($P_{CHO.CHO}$) (excluding potential primary sources) comes from the oxidation of biogenic VOCs such as isoprene, and to a lesser extent monoterpenes, which account in total for 65–70% of the total $P_{CHO.CHO}$ (Fu et al., 2008; Myriokefalitakis et al., 2008). It should be noted

ACPD
9, 8993–9042, 2009

though, that given the large uncertainty of estimates for the isoprene emission flux (280–850 Tg y^{-1}; Wiedinmeyer et al., 2004; Guenther et al., 2006) $P_{CHO.CHO}$ (isoprene) has a large range. The same modeling studies point out that a significant portion of the $P_{CHO.CHO}$ originates from anthropogenic sources; the oxidation of acetylene is the largest anthropogenic source of CHO.CHO accounting for 17–24% of the $P_{CHO.CHO}$. Other anthropogenic sources are the oxidation of the aromatic VOCs, such as benzene, C_6H_6, toluene, C_7H_8 and xylene C_8H_{10}, which are believed to be responsible for 5–11% of $P_{CHO.CHO}$. Additionally, non-negligible VOCs contributing to $P_{CHO.CHO}$ are the ethylene, C_2H_4 and propylene, C_3H_6, which account for 2–7% of the global CHO.CHO source. In contrast, the $P_{CHO.CHO}$ from unsaturated γ dicarbonyls, phenols and furanones appears to be negligible (Volkamer et al., 2001; Bloss et al., 2005). Additional sources of CHO.CHO may come from the aqueous oxidation of glycolaldehyde (in addition to the oxidation of other aldehydes) (Lim et al., 2005; Warneck et al., 2005). Other minor contributors are described within Fu et al., (2008) and Myriokefalitakis et al., (2008) (and references cited therein).

1.3 CHO.CHO sinks

CHO.CHO is removed from the atmosphere via a variety of processes. The dominant sink is photolysis (Fu et al., 2008; Myriokefalitakis et al., 2008). Somewhat dependent on the modeling study, the oxidation of CHO.CHO initiated by OH radicals appears to be the next most important sink of CHO.CHO. Another important CHO.CHO sink is its potential role in the formation of secondary organic aerosol, SOA. Chamber experiments by Liggio et al., (2005a,b) showed that the uptake coefficient of the first order irreversible uptake of CHO.CHO by aqueous particles is about 10^{-3}. In contrast, Kroll et al., (2005), pointed out that the particle growth did not occur while CHO.CHO was still present in the gas phase. This finding suggests that the uptake is reversible with no net contribution to SOA formation. More recently, a study (Volkamer et al., 2007) suggested that, lower experimental mixing ratios of CHO.CHO in comparison to those predicted by the Master Chemical Mechanism, (Bloss et al., 2005) above Mexico City

result from a missing sink: CHO.CHO being lost to SOA.

In addition, CHO.CHO can be removed by wet and dry deposition which together account for 9–15% of the total losses (Fu et al., 2008; Myriokefalitakis et al., 2008). In both studies the global estimate of the computed chemical lifetime of CHO.CHO, based on the above mentioned sources and sinks, was, on average, about 3 h. This means that CHO.CHO is short lived. The magnitude of the CHO.CHO amount in an air mass is therefore a surrogate for the oxidation rate of VOCs. As the overwhelming majority of the VOC sources are close to the surface, the CHO.CHO in the boundary layer will dominate the column amount of CHO.CHO. Therefore CHO.CHO columns surrogate for the rate of VOC oxidation and large CHO.CHO columns can be used as a marker of air masses, which are photochemical "hot spots".

Previously, HCHO has been successfully used as an indicator of photochemical oxidation (e.g. Palmer et al., 2003; 2006; Wittrock et al., 2006; De Smedt et al., 2008; Müller et al., 2008). CHO.CHO is arguably a better indicator of the rate of photochemical processing, because unlike HCHO it is not produced in the oxidation of methane, CH_4. In addition the lower primary vehicle emissions of CHO.CHO as compared to those of HCHO, make CHO.CHO a better indicator for the oxidation of the anthropogenic VOCs in air masses polluted by traffic.

1.4 Importance

The aim of this study is to provide information on the spatial distribution, and the temporal evolution of CHO.CHO as observed for the period 1 August 2002–31 December 2007, using measurements of the solar back scattered electromagnetic radiation upwelling from the top of the atmosphere by space based instrumentation. Inversion of these data yields observations of the temporal and spatial variation of CHO.CHO. This, as already discussed, improves and tests our knowledge of the processes controlling the oxidizing capacity of the troposphere and also constrains our understanding on the different sources of emissions and their magnitude.

In the first section of this manuscript, the satellite instrument, the retrieval approach

ACPD
9, 8993–9042, 2009

and the methods used to determine the atmospheric columns of CHO.CHO are described. This is followed by a comparison of the CHO.CHO columns retrieved in this way with the in situ ground-based observations of CHO.CHO found in the literature. Afterwards, the distribution of the vertical column densities of CHO.CHO is analyzed in terms of both spatial and temporal variability on i) a global scale and ii) over selected regions where high CHO.CHO values are encountered. The synergistic use of other short lived trace gas observations, such as HCHO and nitrogen dioxide, NO_2, to characterize the origins of CHO.CHO, i.e. emissions linked to anthropogenic activities, biogenic processes and biomass burning sources, is discussed.

2 Instrumentation and methods

2.1 The SCIAMACHY instrument

The SCIAMACHY (SCanning Imaging Absorption spectroMeter for Atmospheric CartograpHY) is an imaging UV-VIS-near IR spectrometer, mounted on the ESA ENVISAT satellite, which was launched on the 28 February 2002. SCIAMACHY's primary mission goal is to measure trace gases, clouds and aerosol properties, in the troposphere and stratosphere. To achieve this, SCIAMACHY measures the transmitted, reflected and scattered light upwelling at the top of the atmosphere from the Earth's atmosphere and surface (Burrows et al., 1995; Bovensmann et al., 1999; Gottwald et al., 2006). ENVISAT flies in a sun synchronous, near polar orbit with a local equator crossing time of 10:00 a.m. in the descending node. It has three viewing geometries (Nadir, Limb and Solar Occultation). For the current study, the nadir mode having a spatial resolution of 30 km along track and 60 km across track (60×30 km) was used. Global coverage is achieved for this viewing mode in about six days.

ACPD
9, 8993–9042, 2009

2.2 The retrieval method – DOAS technique and the CHO.CHO algorithm

CHO.CHO spectral bands

The highly resolved CHO.CHO absorption cross section (FWHM=0.001 nm) (Volkamer et al., 2005) has been convolved with the SCIAMACHY spectral response, known as slit function (Fig. 1a). CHO.CHO has strong absorption bands in the blue wavelength region (420–460 nm). The relatively strong CHO.CHO feature peaking at 455 nm and several other characteristic, but smaller features (e.g. at 440 nm) are included in the wavelenght window, chosen for the retrieval. The maximum absorption cross section value of this sharp CHO.CHO peak (at 455 nm) is $\sigma_{(CHO.CHO)}=5.45\times10^{-19}$ cm^2 molec^{-1}.

These characteristic bands were recently used to retrieve CHO.CHO locally (e.g. Sinreich et al., 2007) as well as globally from space (Wittrock et al., 2006). The sharp and characteristic features of CHO.CHO absorption spectra are ideal for the use in the retrieval technique known as the differential optical absorption spectroscopy (DOAS), (Platt and Perner, 1980; Platt, 1994).

2.3 DOAS technique and the retrieval of the slant column densities of CHO.CHO

DOAS, is a technique used for the discrimination of the characteristic higher frequency absorption structures of trace gases from the slowly varying broad band extinction processes such as Rayleigh and Mie scattering and broad band molecular absorption, as well as potential instrumental artifacts. To do so, a high pass polynomial filter, accounting for these broad band structures, is applied. The higher frequency spectral features are used to retrieve the trace gases absorptions known as slant column absorptions. These are converted to Slant Column Densities (SCD) by taking into account the relevant absorption cross sections. SCDs represent the amount of the trace gas along the average path taken by photons, during their travel through the atmosphere and back to the satellite sensor. The quantitative determination of the SCDs is achieved by applying a non linear least square fitting procedure.

ACPD
9, 8993–9042, 2009

For the CHO.CHO retrieval the spectral window of 435–457 nm has been chosen. The reason for excluding the spectral features of CHO.CHO around 420 nm is a large interference with Ring structures. These Ring structures arise from the infilling of Fraunhofer features in the scattered electromagnetic radiation by rotational Raman scattering on air molecules. The chosen wavelength window was found to be the optimal in terms of achieving reasonably small residuals and a good sensitivity to CHO.CHO. The reference absorption cross sections that were used in the retrieval process include CHO.CHO (Volkamer at el., 2005), and interfering species such as O_3 (Bogumil et al., 1999), NO_2 (Bogumil et al., 1999), O_4 (O_2-O_2 collision) (Greenblatt et al., 1990), water vapor (HITRAN database, http://www.cfa.harvard.edu/hitran/), the pseudo-absorption features due to Rotational Raman Scattering (RRS) by air molecules (Ring effect, Vountas et al., 1998), the absorption of phytoplankton (Bracher and Tilzer, 2001; Vountas et al., 2007) and also a 4th order polynomial. Figure 1b shows a representative example of a DOAS fit of CHO.CHO for a ground scene above a smoke plume observed during intensive biomass burning above Greece, in August 2007. The blue dotted line shows the CHO.CHO fitted result after removing all other absorbers. The black line depicts the scaled laboratory reference. The computed $SCD_{CHO.CHO}$ for this case was 6.23×10^{15} molec cm^{-2}, the estimated fitting error 7.9%, with the chi-square value 5.1×10^{-6}.

The next step in the retrieval process is to account for clouds. Only the ground pixels having cloud coverage less than 20% were considered by applying an intensity filter criterion. It should be noted that the residual clouds may lead to an underestimation of the CHO.CHO columns.

2.4 Air mass factors and vertical column densities computation

The obtained SCDs are converted to Vertical Column Densities (VCDs) after applying the air mass factors (AMF), which, in mathematical terms is defined as the ratio of the SCD/VCD and depends on the radiative transfer properties of the atmosphere. The AMF is a function of many parameters such as the surface spectral reflectance of the

observed ground scene, the surface pressure, the viewing geometry, the clouds, the aerosol vertical distribution and its optical thickness, the solar zenith angle and finally, the vertical distribution of CHO.CHO in the lowermost troposphere. For this study, the block air mass factors from Wittrock, (2006) were used. These AMF computations were conducted with the radiative transfer model SCIATRAN (Rozanov, 2005 and references therein), which takes into account all the above mentioned parameters. The resultant global annual mean composite CHO.CHO air mass factors are shown in Fig. 2b. As illustrated in this figure, the mean value of AMF, on a global scale is about 2. There are several regions, where this value is lower as for example where the visibility is reduced significantly (e.g. above areas of biomass burning and industrialized areas) or higher due to a high albedo (e.g. Polar Regions).

2.5 CHO.CHO detection limit and error analysis

For cloud free scenes, the accuracy of the Vertical Column Densities of CHO.CHO retrieved from SCIAMACHY measurements depends on several individual errors which can be systematic and/or random in origin.

The systematic errors comprise the

1. error on the knowledge of the trace gas absorption cross sections and their temperature dependence
2. the atmospheric temperature
3. instrumental errors (e.g. wavelength calibration),
4. errors in air mass factor calculations, offset errors and
5. correlation errors (e.g. interference with Ring spectral features).

Most of these errors are estimated to be in the order of a few percent (Wittrock, 2006).

The random errors comprise the noise on the measured backscattered electromagnetic radiation as a function of wavelength range relative to the measured absorption.

ACPD
9, 8993–9042, 2009

In order to calculate the detection limit of the slant column densities the simple approximation of an ideal measurement is considered; the SCD should be at least larger than the ratio of the root mean square noise (RMS) of the optical density, $(\ln(I_0//))$, to the absorption cross section of the species of interest,

$$\mathrm{SCD}_{\mathrm{lim}} \geq \frac{\mathrm{RMS}}{\sigma_{\mathrm{CHO.CHO}}} .$$

The typical RMS value of SCIAMACHY at the wavelength region of 450 nm is 3.3×10^{-4}. Taking into account that the maximum absorption cross section of CHO.CHO is $\sigma_{(\mathrm{CHO.CHO})}=5.5\times10^{-19}\,\mathrm{cm}^2\,\mathrm{molec}^{-1}$ the individual slant column density limit is $6.0\times10^{14}\,\mathrm{molec\,cm}^{-2}$. It should be noted that the systematic error based on the estimations of Wittrock, 2006 is about $4.0\times10^{14}\,\mathrm{molec\,cm}^{-2}$. The random limit reduces when averaging in space and time, assuming Poisson statistics.

Nevertheless this averaging has a direct impact on the spatial and temporal resolution of the data. For this study, the monthly means of $\mathrm{VCD}_{\mathrm{CHO.CHO}}$ were used. For these monthly composites of cloud free scenes (cloud fraction <20%) the total uncertainty is given by:

$$[2 \times 10^{14} + X \cdot \mathrm{VC}_{\mathrm{CHO.CHO}}]\,(\mathrm{molec\,cm}^{-2})$$

The additive term is determined by the minimum detectable absorption of CHO.CHO assuming non-systematic errors only. The value of X is strongly ground scene dependent but varies typically in the range 0.1 to 0.3. A detailed description of the systematic error sources is presented elsewhere (Wittrock, 2006; Wittrock, et al., 2006).

3 Results and discussion

3.1 Global $\mathrm{VCD}_{\mathrm{CHO.CHO}}$ levels

In the current study, a data set comprising more than five years (August 2002–December 2007) of SCIAMACHY observations of CHO.CHO has been generated. As

the stratospheric column of CHO.CHO is negligible, this data set represents the tropospheric $VCD_{CHO.CHO}$. Figure 2a and b shows the CHO.CHO slant column densities and the air mass factors used in this study to determine the VCD. For both figures the multi-annual average for the time span of 2003–2007 has been taken into account to obtain five complete years of measurements.

Enhanced CHO.CHO column amounts of $SCD_{CHO.CHO} \geq 1.2 \times 10^{15}$ molec cm^{-2} (Fig. 2a) and $VCD_{CHO.CHO} \geq 6 \times 10^{14}$ molec cm^{-2} (Fig. 2c) have been observed. The majority of the areas, having enhanced CHO.CHO columns are in tropical and subtropical regions. South America, Africa, India, Indonesia and Asia (mainly South-Eastern China) are among the regions, where high values of CHO.CHO are retrieved. At middle latitudes, moderate values of $VCD_{CHO.CHO}$ of about 3×10^{14} molec cm^{-2} are discernible, for example above North America, Europe and Australia. Notably, high column amounts of CHO.CHO are also found above water, close to upwelling areas and regions having significant amounts of phytoplankton as indicated by their ocean colour. This implies oceanic biogenic activity as a possible source of CHO.CHO precursors (This is discussed further in Sect. 3.5.7).

Due to the short lifetime of CHO.CHO of about 2–3 h, these high values are expected to originate mostly from regional sources of the precursor VOCs. Indeed, as it will be described later on (Sect. 3.5) depending on the season, these regions are characterized by strong biogenic emissions, biomass burning and pollution induced from anthropogenic activities.

3.2 Comparison of space observations and ground based measurements

A comparison of the data set of the CHO.CHO, retrieved from SCIAMACHY with the ones published involving in situ ground based measurements was undertaken in this study. In Table 1 the CHO.CHO mixing ratios reported in the literature are compiled. The air masses over these measuring sites are characterized as polluted-urban, polluted semi-urban, rural (sometimes influenced by urban plumes) and maritime. Unfortunately, no observations are available for the southern hemisphere, where high

ACPD
9, 8993–9042, 2009

concentrations of CHO.CHO are observed from space.

In order to compare directly the in situ measurements of CHO.CHO mixing ratios with the space based observations of tropospheric columns of CHO.CHO several assumptions had to be made. For example, it has been assumed that CHO.CHO is well mixed inside the boundary layer which has been calculated from the *LMDz-INCA* model for the year 2000 (K. Tsigaridis, personal communication). For the conversion of the vertical column densities, standard conditions of temperature and pressure (25 °C and 1 atm) have been used.

The spatial resolution of the SCIAMACHY instrument (30×60 km) is large in comparison to the point of the in-situ measurements. We assume for the present that the point measurements are representative for a box of dimensions 1°×1° surrounding each station.

Finally, the in situ observations were considered to be representative for the whole season that they were conducted, regardless of the actual year of measurements. The reasons are that i) the time series of the SCIAMACHY CHO.CHO data set is limited from August 2002 and on so no direct comparison is feasible with the older in situ datasets and ii) the satellite overpass above a specific point occurs only a few times per month and averaging of data is necessary.

The outcome of the comparison is visualized in Fig. 3. As depicted in this figure, there is a reasonable agreement of the SCIAMACHY observations (red bars) with the ground based observations (blue bars) when taking into account their range (cyan columns), their standard deviation, the numerous assumptions made and the different techniques used. In most of the cases SCIAMACHY overestimates the in situ measurements which would be explained by the transport of CHO.CHO above the boundary layer over constant sources e.g. isoprene emissions over the rural stations. There are a few cases, above urban areas, where SCIAMACHY underestimates the measurements and this could be due to the dilution of the localized anthropogenic emissions to the 1°×1° box chosen for the SCIAMACHY analysis. Interestingly, SCIAMACHY agrees well with the moderate values observed over the ocean (Zhou et al., 1990; Sinreich et

ACPD
9, 8993–9042, 2009

al., 2007) and the only reported aircraft observations, of CHO.CHO mixing ratios (Lee et al., 1998) over Nashville, USA.

3.3 Interannual variability of CHO.CHO vertical column densities

The global distribution of the yearly averaged CHO.CHO columns between 2003 and 2007 is displayed in Fig. 4. A similar pattern is observed, systematically, every year. Each individual composite map of $VCD_{CHO.CHO}$ confirms that, high column amounts are found above regions with dense vegetation (e.g. the tropical forest of Amazonia), biomass burning (e.g. the sub-Saharan Africa) and anthropogenic emissions (e.g. Guangzhou, China) and those having mixtures of these three sources of VOC. A linear regression of the annual averages of tropospheric CHO.CHO was calculated and is plotted in Fig. 5a in addition to the absolute difference of $VCD_{CHO.CHO}$ for the period 2003 to 2007 (Fig. 5b). The calculated detection limit for the average annual changes is about 2.5×10^{13} molec cm^{-2} y^{-1} based on the monthly value (2×10^{14} molec cm^{-2}) and the reduction due to the temporal $\left(\sqrt{\left(\frac{1}{12}\right)}\right)$ and spatial $\left(\sqrt{\left(\frac{1}{4}\right)}\right)$ averaging used.

Above East Asia and mainly China, the calculated difference of the $VCD_{CHO.CHO}$, for the years 2003 to 2007, shows a significant increase (up to 3×10^{14} molec cm^{-2}) as depicted by the red color (Fig. 5b). The linear regression applied to the yearly-based data revealed an annual increase up to 5×10^{13} molec cm^{-2} y^{-1} (Fig. 5a). This increase is found in the same region where an increase in the tropospheric NO_2 column amounts was observed during the period 1996–2004 over the same region (Richter et al., 2005) and which is still increasing. This implies that either an increase in the anthropogenic VOC precursors of CHO.CHO has occurred or there is a potential unknown direct emission of CHO.CHO, most likely originating from anthropogenic activities.

There are other places where the column amounts of CHO.CHO increase or decrease to a significant extent but less than in China. For example a local decrease of CHO.CHO (~3×10^{13} molec cm^{-2} y^{-1}) is found over the tropical forests of Congo at Central Africa. As the length of the data set is increasing, our knowledge of the signifi-

ACPD
9, 8993–9042, 2009

cance of the local and regional changes in CHO.CHO column will improve.

3.4 Seasonal variability of CHO.CHO vertical column densities

The monthly seasonal mean values of the $VCD_{CHO.CHO}$ data set are presented in Fig. 6a. As illustrated in these maps, CHO.CHO VCDs vary according to season. For the majority of the continental areas of both hemispheres, the highest amounts of CHO.CHO are observed during their respective summer and the lowest during winter. In general this behaviour can be explained by 1) enhanced biogenic emissions during the warm periods (Guenther et al., 2006) 2) enhanced amounts of oxidants during summer (Rohrer and Berresheim, 2006; Vrekoussis et al., 2004, 2007; Myriokefalitakis et al., 2008) and 3) overall an increase in the rate of oxidation of the emitted VOCs. The latter reflects, once more, the photochemical origin of CHO.CHO. The pyrogenic emissions of VOC and CHO.CHO also contribute significantly to the observed seasonality as noted in the case of Africa, Amazonia and Indonesia.

In order to better illustrate the general pattern of the seasonal changes observed in the NH and the SH, the "normalized" $VCD_{CHO.CHO}$ have been calculated for selected hot spot areas (1, 4, 9, 10, 11 and 12 for the NH and 2, 3, 6, 7 and 8 for the SH) depicted in Fig. 7 and presented in detail in the next section. The normalized $VCD_{CHO.CHO}$ values are derived from the monthly averages through devision by the annual mean value, e.g. the normalized $VDC_{CHO.CHO}$ for January is calculated from Eq. (1)

$$\text{normalized VCD}_{(\text{Jan})} = \frac{\sum_i^j (\text{VCD}_{(\text{Jan})}/\bar{N}_i)}{(j - i + 1)} \,. \quad (1)$$

In this equation, i is the initial year of measurements, j the end year, and $\bar{N}_i$ the annual average. The use of the normalized values reduces the month-to-month variability caused by the variation in the sources contributing to CHO.CHO production, e.g. an unexpected intensive biomass burning event.

The results of these calculations (Fig. 6b) confirms the above finding, that the CHO.CHO column amount has a strong seasonal variation with the highest values

ACPD
9, 8993–9042, 2009

observed during the warm periods namely June to September for the NH (black circles) and November to February for the SH (Red empty circles). Depending on the sources and the differences in temperatures, the amplitude of those patterns may vary significantly (see Sect. 3.5).

3.5 Photochemical "hot-spot" areas of $VCD_{CHO.CHO}$ – seasonal variability

After focusing on the global composite map of CHO.CHO column amount and its normalized seasonality, the next objective addresses selected specific areas of interest, where the highest values of CHO.CHO columns are observed.

To perform this analysis, twelve "hot-spot" locations (Fig. 7, black boxes) were selected. These locations are presented in Table 2 together with the median VCDs computed for CHO.CHO and HCHO, the average Enhanced Vegetation Index (EVI) (http://earthobservatory.nasa.gov/Observatory/) and the sum of the fire counts based on the analysis of the Advanced Along Track Scanning Radiometer, AATSR instrument (ATSR World Fire Atlas, http://dup.esrin.esa.int/ionia/wfa/index.asp). It should be noted that all the datasets were gridded to the same resolution ($0.5^{\circ}\times0.5^{\circ}$). The respective results are discussed by region in the following subsections in conjunction with both their local seasonality and their interannual variability.

3.5.1 North America

The highest mean values of the VCDs of CHO.CHO over North America, NA, are observed above the Southern East Coast. This region, which is known to have a large biogenic emission, is characterized by enhanced EVI values, which is directly related to the photosynthetic capacity and primary productivity of the plant canopies.

Over the region defined as NA (Fig. 7 – box 1) the $VCD_{CHO.CHO}$ have a median annual value equal to 3.7×10^{14} molec cm^{-2} which on average vary between low values in winter (2.5×10^{14} molec cm^{-2}) up to about 5.0×10^{14} molec cm^{-2} in summer following the changes of the EVI (green line). The seasonal behaviour of the CHO.CHO values,

ACPD
9, 8993–9042, 2009

as already pointed out, can be attributed to the oxidation of biogenic VOCs (bVOCs) such as isoprene (Wiedinmeyer et al., 2005) and terpenes. The oxidation of VOCs will lead also to high values of the column amount of HCHO, which is a major product of the oxidation scheme of isoprene (Spaulding et al., 2003 and references therein).

Indeed and in agreement with the above assumptions, both the terrestrial isoprene emissions (Guenther et al., 2006) and the respective VCD_{HCHO} observations (Chance et al., 2000; Abbot et al., 2003; Wittrock, 2006; De Smedt et al., 2008; Stavrakou et al., 2008) show enhanced values above the Southern East Coast. The ratio 0.044±0.009 computed from the annual mean values of $VCD_{CHO.CHO}/VCD_{HCHO}$, defined as R_{GF}, agrees with the mean value of 0.045 found during the SCAPE experiment (Munger et al., 1995) held at the mountain ridge site in Shenandoah National Park, Virginia.

Several other spots with high CHO.CHO values are revealed when looking across the NA continent. These are mainly influenced by anthropogenically emitted VOCs, e.g. above Los Angeles at the West Coast, where on average $VCD_{CHO.CHO} \geq 5.8 \times 10^{14}$ molec cm^{-2} are found. The analysis of these more localized phenomena will be described in a forthcoming publication.

3.5.2 South America

As depicted in Fig. 7b, the highest $VCD_{CHO.CHO}$ are computed over the tropical rainforests of Amazonia. The abundance of CHO.CHO in this region is controlled not only by VOCs induced by biogenic sources (high values of EVI, Table 2) but also by biomass burning emission (Table 2). Although fires contribute less systematically than the biogenic emissions, their occurrence coincides with high amounts of CHO.CHO. This is confirmed from the analysis of the VCDs of CHO.CHO for boxes 2 (central and western SA) and 3 (eastern SA) presented in Fig. 7.

Here both the EVI and the calculated number of fires are high (Table 2). Nevertheless the relative importance of fires depends on the total area of the chosen regional boxes. Thus, taking into account that box 2 is about seven times larger than box 3, it is clear that fires affect more drastically box 3. In addition, box 3 is a region where almost all fire

ACPD
9, 8993–9042, 2009

events occur during the period July–October while box 2 encounters two fire seasons with the maxima of the fire counts observed in March and in September.

For the region 2, the median $VCD_{CHO.CHO}$ equals 5.3×10^{14} molec cm^{-2}. When focusing on the smaller box an increase of 25% is found in CHO.CHO. Interestingly the increase in HCHO is smaller (10%) which implies that CHO.CHO, at least for this specific case study, might be a more sensitive metric for monitoring the air quality above biomass burning. The difference in the increase of the concentrations of those species results in slightly higher CHO.CHO/HCHO ratio of the mean VCDs (R_{GF}=0.049±0.016) calculated for the small region in comparison to the respective one characterizing the larger region (R_{GF}=0.045±0.012). The annual mean VCDs of NO_2 remain quite low for both regions with the respective values being equal to $3–4\times10^{14}$ molec cm^{-2}.

Interestingly, although the strength of the apparent sources of precursor VOCs linked to CHO.CHO production at both coherent regions are different, the seasonal variability (Fig. 7 – boxes 2 and 3) is showing that the maxima are found during the same period around November and the minima around July.

For the larger area (box 2) this is supported by the findings of Huete et al. (2006), who observed a progressive increase of the EVI in Amazonia during the dry season (July–mid November). The same period coincides with the fire season affecting mainly the selected region 3 in addition to the impact of the local vegetation. The biomass burning in this case has a direct effect in the reported amplitude (Fig. 7 – box 3) of the mean variability of CHO.CHO which in total is enhanced by 85%.

3.5.3 Africa

Africa is one of the continents where some of the highest CHO.CHO VCDs are observed. The reason is that as in the case of S. America, Central Africa is covered with dense vegetation, which have large emission of VOC and in addition biomass burning is a regular reoccurring phenomena. To the north and south of the tropical forests, the vegetation type changes to deciduous forests and savannas. In addition to these strong biogenic emissions, CHO.CHO is produced from wild fires and savan-

ACPD
9, 8993–9042, 2009

nan fires (Cahoon et al., 1992). These fire events are seasonally dependant as it is shown not only from the ATSR world fire atlas but also from the respective carbon monoxide, CO from Mopitt (Measurements of pollution in the Troposphere, MOPITT, http://web.eos.ucar.edu/mopitt/index.html) and SCIAMACHY (Buchwitz et al., 2007). In West Africa fires peak from December to February and in Southern Africa during May–August (Fig. 7, red columns). This should result in different patterns in the observed seasonality. Indeed, and as depicted in Fig. 7, in regional boxes 4 and 6, the seasonal variation of CHO.CHO is shifted by a 6 month time span following the peak of the fires.

Moving from the northern hemisphere to the southern hemisphere for the selected regions in Fig. 7, a gradual decrease in CHO.CHO amounts, is observed. The median VCD values are 5.8, 5.4 and 5.1×10^{14} molec cm^{-2} for the boxed areas 4, 5 and 6, respectively. Each of the three regions is controlled by different types and mixtures of emissions.

The 4th box, at the north west of the major tropical forest area is populated mostly with deciduous humid forests, derived Savanna and partially with tropical forests at its coastal borders to the south. The total amount of biomass burned in this region is the largest for the entire continent (Hao and Liu, 1994). Climatologically, there is a well distinguished "wet – dry" system characterizing this area. CHO.CHO VCDs obtain their highest values (Fig. 7 – box 4) from December to February when the peak of fires is observed. An increase is observed from July. This behaviour can be explained by the high EVI values, implying large biogenic emissions and the ensuing photochemistry during summer. The computed ratio R_{GF} is equal to 0.050±0.006.

Box 5 is covered completely by tropical forest with wild fires occurring sporadically. The climate is tropical with fairly constant temperatures (around 27°C) corresponding to two dry and two wet season (Stavrakou et al., 2008). Small changes are found for the month-to-month variability of CHO.CHO (Fig. 7 – box 7) and the R_{GF} was 0.043±0.004, a value close to the one already calculated over the biogenically influenced areas.

Finally, box 6 is covered by mid sub-humid wooden savannas and the climate is

ACPD
9, 8993–9042, 2009

similar to the one mentioned for region 4. The observed contrary seasonality is linked to the pyrogenic emissions occurring during the dry season which in this case peaks in August. The retrieved CHO.CHO has a two maxima shape with the highest values computed in August due to the fires, and the second in December due to the enhanced biogenic emissions. The R_{GF} is in this case equal to 0.046±0.004 slightly higher than the one of box 5.

3.5.4 Europe

Over Europe the values of the CHO.CHO columns are moderate. Above the selected areas in Western Europe the anthropogenic sources are of major importance as expressed by the high NO_2 vertical columns (Richter et al., 2005). The monthly mean CHO.CHO columns range from 1.5×10^{14} molec cm^{-2} in winter to 3.0×10^{14} molec cm^{-2} in summer (Fig. 7 – box 12) and the median annual value is 2.2×10^{14} molec cm^{-2}. The respective HCHO columns over the same region are also moderate and their median value is found to be equal to 7.3×10^{15} molec cm^{-2}. The ratio of both trace gases in this case is R_{GF}=0.035±0.007 suggesting that over anthropogenically influenced regions the ratio decreases as a result of higher primary sources of HCHO in comparison to the CHO.CHO ones (Garcia et al., 2006). Another indirect source of HCHO but not of CHO.CHO comes from the decomposition of the peroxyacetyl nitrate (PAN), a product of the photochemical reaction of VOCs and NO_2. The thermal decomposition of PAN has a relatively large enthalpy resulting in a strong temperature dependence. PAN is therefore a temporary reservoir for HCHO.

3.5.5 Asia

Four hot spots are selected over Asia. One is found over India, one in Indonesia and two over China.

Both the southern and northern China regions (Fig. 7 – boxes 9 and 10) regions are controlled by strong biogenic as well as pyrogenic emissions (Fu et al., 2007;

ACPD
9, 8993–9042, 2009

Stavrakou et al., 2008). The northern region is additionally fingerprinted by large agricultural biomass burning which maximizes in June (Fu et al., 2007) and with rapidly increasing anthropogenic emissions (Richter et al., 2005). The median annual value of the $VCD_{CHO.CHO}$ is higher for the southern box (5.8×10^{14} molec cm^{-2}) in comparison to the northern (4.5×10^{14} molec cm^{-2}).

The seasonal pattern is relatively similar for both areas, with the maximum values being retrieved during summer but a second increase, found in March until July for the southern region. This increase has been observed also, in the HCHO values (Fu et al., 2007; Stavrakou et al., 2008). The calculated R_{GF}s are 0.046±0.005 and 0.039±0.005 for the southern and the northern boxes, respectively. The values of the median VCD_{NO_2} were almost 5 times larger over the northern China suggesting, as in the case of Europe, that the lowest values of R_{GF} occur over areas where anthropogenically induced emissions from fossil fuel combustion occur.

In India the selected hot spot is located above a densely populated area (http://earthobservatory.nasa.gov/IOTD/view.php?id=432 close to the Himalaya Mountains. The seasonality of CHO.CHO follows the northern hemispheric pattern with the maxima found in summer (Fig. 7 – box 11). The median annual value was equal to 4.9×10^{14} molec cm^{-2} and the computed R_{GF} was 0.053±0.008. These numbers point to the existence of supplementary sources of CHO.CHO in addition to the biogenic emissions occurrence. Another major source of NMVOCs in India are the residential emissions (wood fuel), as reported in the Emission Database for Global Atmospheric Research (EDGAR). The relatively low median NO_2 VCDs (2.5×10^{15} molec cm^{-2}) over box 11 agrees with the findings of the EDGAR database stating that the pollution induced from industrialization processes currently is not the key contributor to NMVOC production.

Over Indonesia (Fig. 7 – box 7), the annual cycle in CHO.CHO is less profound. Higher mean VCDs are observed from September to February and lower columns from March to August. The median $VCD_{CHO.CHO}$ was 5.5×10^{14} molec cm^{-2} and the reported R_{GF} of 0.068±0.039 was not only the highest among all the studied values of the 12

ACPD
9, 8993–9042, 2009

hot spots but also the one with the greatest variability. At first glance, this appears to be linked with increased biomass burning, which can be supported by the conditions occurring in this region. Indonesia is covered by tropical forests. Climatologically, it is affected by a dry monsoonal period mainly between July and October. During this period, fires are placed for agricultural land clearing and deforestation. In parallel, wild fires occur at the tropical forests due to the dry climate (Murdiyarso and Adiningsih, 2006). In addition Indonesia is one of the regions suffering from the drier conditions caused by the El-Niño phenomenon and subsequently the increase of fire numbers. As seen in Fig. 7 – box 7 (blue dashed line), the monthly averages of the $VCD_{CHO.CHO}$ were up to 27% higher in 2006, a characteristic El-Niño year, in comparison to the data excluding the El-Nino year (not shown here), during October and November.

3.5.6 Australia

Northern Australia is also characterised by biogenic emissions and periods of biomass burning. Both contribute to the observed seasonal cycle, which minimizes during the cold period (June-July-August) due to the absence of precursors in addition to lower photochemistry. During the fire season (July–December) CHO.CHO columns exhibit a sharp increase $4–5\times10^{14}$ molec cm^{-2}, which ends in February when the maximum EVI values are obtained (Fig. 7 – box 7). The observed ratio of CHO.CHO to HCHO in this region is 0.059 ± 0.009 indicative of the large numbers of fires occurring in Northern Australia.

3.5.7 Oceanic $VCD_{CHO.CHO}$

The following oceanic $VCD_{CHO.CHO}$ analysis should be treated with care as it is known that trace-gas observations of small absorbers suffer from retrieval artifacts over water (e.g. interference from liquid water absorption) making their interpretation more difficult in comparison to land values.

High $VCD_{CHO.CHO}$ (in some cases $\geq4\times10^{4}$ molec cm^{-2}) are observed at several re-

ACPD
9, 8993–9042, 2009

gions above the ocean (Fig. 2c). The most abundant oceanic regions of CHO.CHO are in the tropics. In addition there is a seasonal modulation of CHO.CHO over the southern oceans and northern ocean. The values of CHO.CHO are less over the higher latitudes but a clear seasonal cycle is observed. The regions, where CHO.CHO is observed above the oceans are known to be biological active: relatively large amounts of phytoplankton monitored from space result to enhanced Oceanic Net Primary Productivity values (npp, http://www.science.oregonstate.edu/ocean.productivity/, based on MODIS chlorophyll and temperature data).

The strong signals in the tropics in particular in the Pacific are affected by the Intertropical Convergence Zone (ITCZ). In this region strong convection occurs lifting moist-air masses having marine aerosol.

The latter is indicative of another potential source of the CHO.CHO over oceans: the convection of organic aerosols, reach in dissolved organic carbon (DOC) to the troposphere. The oceanic and coastal surface microlayers are enriched in low molecular weight carbonyls in comparison to the subsurface water as a result of the enhanced photo-production rate (Zhou and Mopper, 1997). This may facilitate their release to the atmosphere at the surface or from marine aerosol, which is created from wave breaking and foam etc. These aerosols under the presence of oxidants (OH, O_3 and NO_3) and/or halogens may extract the dissolved organic carbon in the form of organic radicals in the gas phase. Possibly a complex process controls the chemical scheme of the production of CHO.CHO from the oceanic sources and further investigation is needed.

The oceanic behavour of CHO.CHO in connection with various oxidants (e.g. O_3, OH, IO) as well as with the observed net primary productivity is subject of a paper in preparation.

3.6 Interannual variability and trends over the hotspot areas

The hot-spots described above are now analyzed in terms of their interannual variability. The individual measurements of $VCD_{CHO.CHO}$ coupled with the respective residual

mean squares (RMS) and the monthly means are illustrated in Fig. 8.

The seasonal patterns emanating from this figure were already described above. In order to observe potential trends for the specific selected hot spots of CHO.CHO, a linear regression analysis has been applied to the results and the outcome is presented separately in Fig. 9.

Four of the twelve hot-spots, NE and SE Asia, India and Australia present an annual increase in CHO.CHO Vertical Column Densities. For Australia, India and SE Asia the annual computed increase of 1.6% and 1.2% and 3.5%, respectively, is small. Notably, during the period 2003–2007, the vertical columns of CHO.CHO increased over NE China by about 45%. This increase is attributed, at least partially to the increase of the VOC emissions following the rapid and continuous economic development of this region (Richter et al., 2005).

On the contrary, a small decrease of 4.0%, 1.3%, 1.7%, 4%, and 3% in the $VCD_{CHO.CHO}$ was found over Western Europe, S. America, and Africa, respectively. Over Western Europe, a 18% NO_x emission reduction, from 1996 to 2002, is also reported (Richter et al., 2005). This reduction in NO_x emissions reflects the decrease of man-made emissions. The decrease of CHO.CHO has to be treated with care as the median value of the $VCD_{CHO.CHO}$ for the studied period is also very low (2.2×10^{14} molec cm^{-2}).

As the length of the data set increases, the significance of the observed changes and any non linear behaviour will become clearer.

4 Conclusions

SCIAMACHY measurements of the upwelling radiance at the top of the atmosphere have been used to obtain the first global multi-annual (2002–2007) dataset of the CHO.CHO vertical column densities. The slant columns were retrieved in the 435–457 nm spectral region using the DOAS technique: slant column densities being initially retrieved and then converted to vertical columns densities by using air mass

ACPD
9, 8993–9042, 2009

factors. The verification and validation of the space-based observations was made using ground-based measurements reported in the literature. Taking into account the assumptions needed to obtain a coherent dataset, the comparisons between ground based and satellite data showed a good agreement within uncertainties.

As CHO.CHO's lifetime is short (about 2–3 h), the column amounts of CHO.CHO can be used as a regional and global marker of photochemical hot-spots, which are defined as regions where photochemical oxidation of chemical species is rapid. Several hot-spots regions were selected and their temporal variation was analyzed. Spatially, the highest values of CHO.CHO VCDs are observed over tropical and sub-tropical regions. South America, Africa, India, Indonesia and Asia (mainly China) have the largest columns of CHO.CHO followed by North America ground scenes, Europe and Australia. Notably, large column amounts of CHO.CHO are also found above the ocean, close to upwelling areas and above regions having large concentrations of phytoplankton suggesting biogenic activity, perhaps coupled with photochemistry as the oceanic source of the CHO.CHO.

The highest CHO.CHO amounts are found over regions controlled by strong biogenic and pyrogenic emissions. The VOCs emitted from those sources act as the precursor "fuel" in the CHO.CHO production. Nevertheless attention should be given to exploit the primary emission of CHO.CHO, linked to the strong biomass burning events.

Temporally, the levels of CHO.CHO vary seasonally due to the changes in the biogenically emitted VOCs, mainly isoprene and the ones originating from man-made fires. Other important factors controlling the seasonality of CHO.CHO are the oxidant levels and the induced photochemical reactions. In general, the highest values of the $VCD_{CHO.CHO}$ are observed for both hemispheres during summer and the lowest during winter.

The reported ratio of the CHO.CHO to HCHO amounts was found to be about 0.045 over the source regions controlled by biogenic sources. When shifting to regions affected additionally by biomass burning an increase of this ratio has been computed. On the contrary the presence of anthropogenic sources has been connected to a de-

ACPD
9, 8993–9042, 2009

crease of the respective ratio possibly due to the additional sources of HCHO. Further temporal and spatial investigation is needed to better characterize this ratio.

Finally, the interannual global analysis showed that over Northeastern China, an increase in CHO.CHO column amounts of about 3.5×10^{13} molec cm^{-2} y^{-1} or else of 45% is found for the period 2003 to 2007.

Acknowledgements. Mihalis Vrekoussis acknowledges the A. v. Humboldt foundation and the European Union (Marie Curie) for the consecutive research fellowships. We appreciate the provision of MODIS data via the internet by NASA/GSFC and ATSR World Fire Atlas. This work has in part been funded by the DLR, the State of of Bremen, and the EU ACCENT Project. The UB thanks the ESA and DLR for the provision of level 0 and level 1 data from SCIAMACHY.

References

Abbot, D. S., Palmer, P. I., Martin, R. V., Chance, K. V., Jacob, D. J., and Guenther, A.: Seasonal and interannual variability of North American isoprene emissions as determined by formaldehyde column measurements from space, Geophys. Res. Lett., 30(17), 1886, doi:10.1029/2003gl017336, 2003.

Bloss, C., Wagner, V., Jenkin, M. E., Volkamer, R., Bloss, W. J., Lee, J. D., Heard, D. E., Wirtz, K., Martin-Reviejo, M., Rea, G., Wenger, J. C., and Pilling, M. J.: Development of a detailed chemical mechanism (MCMv3.1) for the atmospheric oxidation of aromatic hydrocarbons, Atmos. Chem. Phys., 5, 641–664, 2005, http://www.atmos-chem-phys.net/5/641/2005/.

Bogumil, K., Orphal, J., Homann, T., Voigt, S., Spietz, P., Fleischmann, O. C., Vogel, A., Hartmann, M., Kromminga, H., Bovensmann, H., Frerick, J., and Burrows, J. P.: Measurements of molecular absorption spectra with the SCIAMACHY pre-flight model: instrument characterization and reference data for atmospheric remote-sensing in the 230–2380 nm region, J. Photochem. Photobiol. A. Chem., 157, 167–184, doi:10.1016/S1010–6030(03)00062–5, 2003.

Bovensmann, H., Burrows, J. P., Buchwitz, M., Frerick, J., Noel, S., Rozanov, V. V., Chance, K. V., and Goede, A. P. H.: SCIAMACHY: Mission objectives and measurement modes, J. Atmos. Sci., 56, 127–150, 1999.

Bracher, A. U. and Tilzer, M. M.: Underwater light field and phytoplankton absorbance in different surface water masses of the Atlantic sector of the Southern Ocean, Polar Biol., 24, 687–696, 2001.
Buchwitz, M., Khlystova, I., Bovensmann, H., and Burrows, J. P.: Three years of global carbon monoxide from SCIAMACHY: comparison with MOPITT and first results related to the detection of enhanced CO over cities, Atmos. Chem. Phys., 7, 2399–2411, 2007, http://www.atmos-chem-phys.net/7/2399/2007/.
Burrows, J. P., Holzle, E., Goede, A. P. H., Visser, H., and Fricke, W.: Sciamachy – scanning imaging absorption spectrometer for atmospheric chartography, Acta Astronaut., 35, 445–451, 1995.
Cahoon, D. R., Stocks, B. J., Levine, J. S., Cofer, W. R., and Oneill, K. P.: Seasonal Distribution of African Savanna Fires, Nature, 359, 812–815, 1992.
Calvert, J. G., Atkinson, R., Kerr, J. A., Madronich, S., Moortgat, G. K., Wallington, T. J., and Yarwood, G.: The Mechanisms of Atmospheric Oxidation of the Alkenes, Oxford University Press, New York, 2000.
Calvert, J. G., Atkinson, R., Becker, K. H., Kamens, R. M., Seinfeld, J. H., Wallington, T. J., and Yarwood, G.: The Mechanisms of Atmospheric Oxidation of Aromatic Hydrocarbons, Oxford University Press, Oxford, 2002.
Cerqueira, M. A., Pio, C. A., Gomes, P. A., Matos, J. S., and Nunes, T.: Volatile organic compounds in rural atmospheres of central Portugal, Sci. Total Environ., 313, 49–60, doi:10.1016/S0048–9697(03)00250-X, 2003.
Chance, K., Palmer, P. I., Spurr, R. J. D., Martin, R. V., Kurosu, T. P., and Jacob, D. J.: Satellite observations of formaldehyde over North America from GOME, Geophys. Res. Lett., 27, 3461–3464, 2000.
De Smedt, I., Müller, J. F., Stavrakou, T., van der A, R., Eskes, H., and Van Roozendael, M.: Twelve years of global observations of formaldehyde in the troposphere using GOME and SCIAMACHY sensors, Atmos. Chem. Phys., 8, 4947–4963, 2008, http://www.atmos-chem-phys.net/8/4947/2008/.
Fu, T. M., Jacob, D. J., Wittrock, F., Burrows, J. P., Vrekoussis, M., and Henze, D. K.: Global budgets of atmospheric glyoxal and methylglyoxal, and implications for formation of secondary organic aerosols, J. Geophys. Res.-Atmos., 113, D15303, doi:10.1029/2007jd009505, 2008.
Garcia, A. R., Volkamer, R., Molina, L. T., Molina, M. J., Samuelson, J., Mellqvist, J., Galle, B., Herndon, S. C., and Kolb, C. E.: Separation of emitted and photochemical formaldehyde in

Mexico City using a statistical analysis and a new pair of gas-phase tracers, Atmos. Chem. Phys., 6, 4545–4557, 2006, http://www.atmos-chem-phys.net/6/4545/2006/.

Gottwald, M., Bovensmann, H., Lichtenberg, G., Noel, S., von Bargen, A., Slijkhuis, S., Piters, A., Hoogeveen, R., von Savigny, C., Buchwitz, M., Kokhanovsky, A., Richter, A., Rozanov, A., Holzer-Popp, T., Bramstedt, K., Lambert, J.-C., Skupin, J., Wittrock, F., Schrijver, H, and Burrows, J. P.: SCIAMACHY, Monitoring the Changing Earth's Atmosphere; Published by DLR, 2006.

Greenblatt, G. D., Orlando, J. J., Burkholder, J. B., and Ravishankara, A. R.: Absorption-measurements of oxygen between 330 nm and 1140 nm, J. Geophys. Res.-Atmos., 95, 18577–18582, 1990.

Grosjean, D., Grosjean, E., and Gertler, A. W.: On-road emissions of carbonyls from light-duty and heavy-duty vehicles, Environ. Sci. Technol., 35, 45–53, 2001.

Grosjean, E., Grosjean, D., Fraser, M. P., and Cass, G. R.: Air quality model evaluation data for organics. 2. C-1-C-14 carbonyls in Los Angeles air, Environ. Sci. Technol., 30, 2687–2703, 1996.

Guenther, A., Karl, T., Harley, P., Wiedinmyer, C., Palmer, P. I., and Geron, C.: Estimates of global terrestrial isoprene emissions using MEGAN (Model of Emissions of Gases and Aerosols from Nature), Atmos. Chem. Phys., 6, 3181–3210, 2006, http://www.atmos-chem-phys.net/6/3181/2006/.

Hao, W. M. and Liu, M. H.: Spatial and Temporal Distribution of Tropical Biomass Burning, Global Biogeochem. Cy., 8, 495–503, 1994.

Hays, M. D., Geron, C. D., Linna, K. J., Smith, N. D., and Schauer, J. J.: Speciation of gas-phase and fine particle emissions from burning of foliar fuels, Environ. Sci. Technol., 36, 2281–2295, doi:10.1021/Es0111683, 2002.

Houweling, S., Dentener, F., and Lelieveld, J.: The impact of nonmethane hydrocarbon compounds on tropospheric photochemistry, J. Geophys. Res.-Atmos., 103, 10673–10696, 1998.

Huete, A. R., Didan, K., Shimabukuro, Y. E., Ratana, P., Saleska, S. R., Hutyra, L. R., Yang, W. Z., Nemani, R. R., and Myneni, R.: Amazon rainforests green-up with sunlight in dry season, Geophys. Res. Lett., 33, L06405, doi:10.1029/2005gl025583, 2006.

Ieda, T., Kitamori, Y., Mochida, M., Hirata, R., Hirano, T., Inukai, K., Fujinuma, Y., and Kawamura, K.: Diurnal variations and vertical gradients of biogenic volatile and semi-volatile or-

ganic compounds at the Tomakomai larch forest station in Japan, Tellus Series B Chem. Phys. Meteorol., 58, 177–186, doi:10.1111/j.1600–0889.2006.00179.x, 2006.
Jing, L. H., Steinberg, S. M., and Johnson, B. J.: Aldehyde and monocyclic aromatic hydrocarbon mixing ratios at an urban site in Las Vegas, Nevada, J. Air & Waste Manage. Assoc., 51, 1359–1366, 2001.
Kanakidou, M., Seinfeld, J. H., Pandis, S. N., Barnes, I., Dentener, F. J., Facchini, M. C., Van Dingenen, R., Ervens, B., Nenes, A., Nielsen, C. J., Swietlicki, E., Putaud, J. P., Balkanski, Y., Fuzzi, S., Horth, J., Moortgat, G. K., Winterhalter, R., Myhre, C. E. L., Tsigaridis, K., Vignati, E., Stephanou, E. G., and Wilson, J.: Organic aerosol and global climate modelling: a review, Atmos. Chem. Phys., 5, 1053–1123, 2005, http://www.atmos-chem-phys.net/5/1053/2005/.
Kawamura, K., Steinberg, S., and Kaplan, I. R.: Homologous series of C-1-C-10 monocarboxylic acids and C-1-C-6 carbonyls in Los Angeles air and motor vehicle exhausts, Atmos. Environ., 34, 4175–4191, 2000.
Kean, A. J., Grosjean, E., Grosjean, D., and Harley, R. A.: On-road measurement of carbonyls in California light-duty vehicle emissions, Environ. Sci. Technol., 35, 4198–4204, 2001.
Kroll, J. H., Ng, N. L., Murphy, S. M., Varutbangkul, V., Flagan, R. C., and Seinfeld, J. H.: Chamber studies of secondary organic aerosol growth by reactive uptake of simple carbonyl compounds, J. Geophys. Res.-Atmos., 110, D23207, doi:10.1029/2005jd006004, 2005.
Lee, Y. N., Zhou, X. L., and Hallock, K.: Atmospheric carbonyl compounds at a rural southeastern United States site, J. Geophys. Res.-Atmos., 100, 25933–25944, 1995.
Lee, Y. N., Zhou, X., Kleinman, L. I., Nunnermacker, L. J., Springston, S. R., Daum, P. H., Newman, L., Keigley, W. G., Holdren, M. W., Spicer, C. W., Young, V., Fu, B., Parrish, D. D., Holloway, J., Williams, J., Roberts, J. M., Ryerson, T. B., and Fehsenfeld, F. C.: Atmospheric chemistry and distribution of formaldehyde and several multioxygenated carbonyl compounds during the 1995 Nashville Middle Tennessee Ozone Study, J. Geophys. Res.-Atmos., 103, 22449–22462, 1998.
Liggio, J., Li, S. M., and Mclaren, R.: Heterogeneous reactions of glyoxal on particulate matter: Identification of acetals and sulfate esters, Environ. Sci. Technol., 39, 1532–1541, 2005a
Liggio, J., Li, S. M., and McLaren, R.: Reactive uptake of glyoxal by particulate matter. J. Geophys. Res., 110, D10304, doi:10310.11029/2004JD005113, 2005b.
Lim, H. J., Carlton, A. G., and Turpin, B. J.: Isoprene forms secondary organic aerosol through cloud processing: Model simulations, Environ. Sci. Technol., 39, 4441–4446,

doi:10.1021/Es048039h, 2005.
Monks, P. S.: Gas-phase radical chemistry in the troposphere, Chem. Soc. Rev., 34, 376–395, doi:10.1039/B307982c, 2005.
Moortgat, G. K., Grossmann, D., Boddenberg, A., Dallmann, G., Ligon, A. P., Turner, W. V., Gab, S., Slemr, F., Wieprecht, W., Acher, K., Kilber, M., Schlomski, S., and Bachmann, K.: Hydrogen peroxide, organic peroxides and higher carbonyl compounds determined during the BERLIOZ campaign, J. Atmos. Chem., 42, 443–463, 2002.
Müller, K., van Pinxteren, D., Plewka, A., Svrcina, B., Kramberger, H., Hofmann, D., Bachmann, K., and Herrmann, H.: Aerosol characterisation at the FEBUKO upwind station Goldlauter (II): Detailed organic chemical characterisation, Atmos. Environ., 39, 4219–4231, doi:10.1016/j.atmosenv.2005.02.008, 2005.
Müller, J.-F., Stavrakou, T., Wallens, S., De Smedt, I., Van Roozendael, M., Potosnak, M. J., Rinne, J., Munger, B., Goldstein, A., and Guenther, A. B.: Global isoprene emissions estimated using MEGAN, ECMWF analyses and a detailed canopy environment model, Atmos. Chem. Phys., 8, 1329–1341, 2008, http://www.atmos-chem-phys.net/8/1329/2008/.
Munger, J. W., Jacob, D. J., Daube, B. C., Horowitz, L. W., Keene, W. C., and Heikes, B. G.: Formaldehyde, glyoxal, and methylglyoxal in air and cloudwater at a rural mountain site in Central Virginia, J. Geophys. Res.-Atmos., 100, 9325–9333, 1995.
Murdiyarso, D., Adiningsih, E.: Climate anomalies, Indonesian vegetation fires and terrestrial carbon emissions, Mitigat. Adapt. Strateg. Global Change, 12(1), 101–112, doi:10.1007/s11027-006-9047-4, 2006
Myriokefalitakis, S., Vrekoussis, M., Tsigaridis, K., Wittrock, F., Richter, A., Bruhl, C., Volkamer, R., Burrows, J. P., and Kanakidou, M.: The influence of natural and anthropogenic secondary sources on the glyoxal global distribution, Atmos. Chem. Phys., 8, 4965–4981, 2008, http://www.atmos-chem-phys.net/8/4965/2008/.
Palmer, P. I., Jacob, D. J., Fiore, A. M., Martin, R. V., Chance, K., and Kurosu, T. P.: Mapping isoprene emissions over North America using formaldehyde column observations from space, J. Geophys. Res.-Atmos., 108(D6), 4180, doi:10.1029/2002jd002153, 2003.
Palmer, P. I., Abbot, D. S., Fu, T. M., Jacob, D. J., Chance, K., Kurosu, T. P., Guenther, A., Wiedinmyer, C., Stanton, J. C., Pilling, M. J., Pressley, S. N., Lamb, B., and Sumner, A. L.: Quantifying the seasonal and interannual variability of North American isoprene emissions using

satellite observations of the formaldehyde column, J. Geophys. Res.-Atmos., 111, D12315, doi:10.1029/2005jd006689, 2006.
Platt, U. and Perner, D.: Direct Measurements of Atmospheric CH_2O, HN_2, O_3, NO_2, and SO_2 by differential optical-absorption in the near UV, J. Geophys. Res. Oceans Atmos., 85, 7453–7458, 1980.
Platt, U.: Differential optical absorption spectroscopy (DOAS), Air Monitoring by Spectroscopic Techniques, edited by: Sigrist, M. W., John Wiley & Sons, Inc., New York, Vol. 127, pp. 27–84, 1994.
Poisson, N., Kanakidou, M., and Crutzen, P. J.: Impact of non-methane hydrocarbons on tropospheric chemistry and the oxidizing power of the global troposphere: 3-dimensional modelling results, J. Atmos. Chem., 36, 157–230, 2000.
Pope, C. A. and Dockery, D. W.: Health effects of fine particulate air pollution: Lines that connect, J. Air & Waste Manage. Assoc., 56, 709–742, 2006.
Ramanathan, V. and Crutzen, P. J.: New directions: Atmospheric brown "Clouds", Atmos. Environ., 37, 4033–4035, doi:10.1016/S1352–2310(03)00536–3, 2003.
Richter, A., Burrows, J. P., Nuss, H., Granier, C., and Niemeier, U.: Increase in tropospheric nitrogen dioxide over China observed from space, Nature, 437, 129–132, doi:10.1038/Nature04092, 2005.
Roberts, G. C., Artaxo, P., Zhou, J. C., Swietlicki, E., and Andreae, M. O.: Sensitivity of CCN spectra on chemical and physical properties of aerosol: A case study from the Amazon Basin, J. Geophys. Res.-Atmos., 107(D20), 8070, doi:10.1029/2001jd000583, 2002.
Rohrer, F. and Berresheim, H.: Strong correlation between levels of tropospheric hydroxyl radicals and solar ultraviolet radiation, Nature, 442, 184–187, doi:10.1038/Nature04924, 2006.
Rozanov, A., Rozanov, V., Buchwitz, M., Kokhanovsky, A., and Burrows, J. P.: SCIATRAN 2.0 – A new radiative transfer model for geophysical applications in the 175–2400 nm spectral region, Atmos. Remote Sens.: Earth's Surf., Tropos., Stratos. Mesos. – I, 36, 1015–1019, doi:10.1016/j.asr.2005.03.012, 2005.
Seaman, V. Y., Charles, M. J., and Cahill, T. M.: A sensitive method for the quantification of acrolein and other volatile carbonyls in ambient air, Anal. Chem., 78, 2405–2412, doi:10.1021/Ac051947s, 2006.
Sinreich, R., Filsinger, F., Frieß, U., Platt, U., Sebastian, O., Wagner, T., Volkamer, R., and Kern, C.: MAX-DOAS detection of glyoxal during ICARTT 2004, Atmos. Chem. Phys., 7, 1293–1303, 2007,

http://www.atmos-chem-phys.net/7/1293/2007/.
Spaulding, R. S., Schade, G. W., Goldstein, A. H., and Charles, M. J.: Characterization of secondary atmospheric photooxidation products: Evidence for biogenic and anthropogenic sources, J. Geophys. Res.-Atmos., 108(D8), 4247, doi:10.1029/2002jd002478, 2003.
Stavrakou, T., Müller, J.-F., De Smedt, I., Van Roozendael, M., van der Werf, G. R., Giglio, L., and Guenther, A.: Evaluating the performance of pyrogenic and biogenic emission inventories against one decade of space-based formaldehyde columns, Atmos. Chem. Phys., 9, 1037–1060, 2009, http://www.atmos-chem-phys.net/9/1037/2009/.
Tsigaridis, K. and Kanakidou, M.: Global modelling of secondary organic aerosol in the troposphere: a sensitivity analysis, Atmos. Chem. Phys., 3, 1849–1869, 2003, http://www.atmos-chem-phys.net/3/1849/2003/.
Tsigaridis, K. and Kanakidou, M.: Secondary organic aerosol importance in the future atmosphere, Atmos. Environ., 41, 4682–4692, doi:10.1016/j.atmosenv.2007.03.045, 2007.
Tsigaridis, K., Lathiere, J., Kanakidou, M., and Hauglustaine, D. A.: Naturally driven variability in the global secondary organic aerosol over a decade, Atmos. Chem. Phys., 5, 1891–1904, 2005, http://www.atmos-chem-phys.net/5/1891/2005/.
Volkamer, R., Platt, U., and Wirtz, K.: Primary and secondary glyoxal formation from aromatics: Experimental evidence for the bicycloalkyl-radical pathway from benzene, toluene, and p-xylene, J. Phys. Chem. A., 105, 7865–7874, 2001.
Volkamer, R., Spietz, P., Burrows, J., and Platt, U.: High-resolution absorption cross-section of glyoxal in the UV-vis and IR spectral ranges, J. Photochem. Photobiol. A–Chem., 172, 35–46, 2005.
Volkamer, R., Molina, L. T., Molina, M. J., Shirley, T., and Brune, W. H.: DOAS measurement of glyoxal as an indicator for fast VOC chemistry in urban air, Geophys. Res. Lett., 32, L08806, doi:10.1029/2005gl022616, 2005.
Volkamer, R., Martini, F. S., Molina, L. T., Salcedo, D., Jimenez, J. L., and Molina, M. J.: A missing sink for gas-phase glyoxal in Mexico City: Formation of secondary organic aerosol, Geophys. Res. Lett., 34, L19807, doi:10.1029/2007gl030752, 2007.
Volkamer, R., Jimenez, J. L., San Martini, F., Dzepina, K., Zhang, Q., Salcedo, D., Molina, L. T., Worsnop, D. R., and Molina, M. J.: Secondary organic aerosol formation from anthropogenic air pollution: Rapid and higher than expected, Geophys. Res. Lett., 33, L17811,

doi:10.1029/2006gl026899, 2006.
Vountas, M., Rozanov, V. V., and Burrows, J. P.: Ring effect: Impact of rotational Raman scattering on radiative transfer in earth's atmosphere, J. Quantit. Spectrosc. Radiat. Transf., 60, 943–961, 1998.
Vountas, M., Dinter, T., Bracher, A., Burrows, J. P., and Sierk, B.: Spectral studies of ocean water with space-borne sensor SCIAMACHY using Differential Optical Absorption Spectroscopy (DOAS), Ocean Sci., 3, 429–440, 2007, http://www.ocean-sci.net/3/429/2007/.
Vrekoussis, M., Mihalopoulos, N., Gerasopoulos, E., Kanakidou, M., Crutzen, P. J., and Lelieveld, J.: Two-years of NO_3 radical observations in the boundary layer over the Eastern Mediterranean, Atmos. Chem. Phys., 7, 315–327, 2007, http://www.atmos-chem-phys.net/7/315/2007/.
Vrekoussis, M., Kanakidou, M., Mihalopoulos, N., Crutzen, P. J., Lelieveld, J., Perner, D., Berresheim, H., and Baboukas, E.: Role of the NO_3 radicals in oxidation processes in the eastern Mediterranean troposphere during the MINOS campaign, Atmos. Chem. Phys., 4, 169–182, 2004, http://www.atmos-chem-phys.net/4/169/2004/.
Wang, Y. H., Jacob, D. J., and Logan, J. A.: Global simulation of tropospheric O_3-NO_x-hydrocarbon chemistry 3. Origin of tropospheric ozone and effects of nonmethane hydrocarbons, J. Geophys. Res.-Atmos., 103, 10757–10767, 1998.
Wang, Y. H., Logan, J. A., and Jacob, D. J.: Global simulation of tropospheric O_3-NO_x-hydrocarbon chemistry 2. Model evaluation and global ozone budget, J. Geophys. Res.-Atmos., 103, 10727–10755, 1998.
Warneck, P.: Multi-phase chemistry of C-2 and C-3 organic compounds in the marine atmosphere, J. Atmos. Chem., 51, 119–159, doi:10.1007/s10874-005-5984-7, 2005.
Wiedinmyer, C., Guenther, A., Harley, P., Hewitt, N., Geron, C., Artaxo, P., Steinbrecher, R., and Rasmussen, R.: Global Organic Emissions from Vegetation, in: Emissions of Atmospheric Trace Compounds, edited by: Granier, C., Artaxo, P., and Reeves, C., Kluwer Academic Publishers, Dordrecht, The Netherlands, p. 544, 115–170, 2004.
Wiedinmyer, C., Greenberg, J., Guenther, A., Hopkins, B., Baker, K., Geron, C., Palmer, P. I., Long, B. P., Turner, J. R., Petron, G., Harley, P., Pierce, T. E., Lamb, B., Westberg, H., Baugh, W., Koerber, M., and Janssen, M.: Ozarks Isoprene Experiment (OZIE): Measurements and modeling of the "isoprene volcano", J. Geophys. Res.-Atmos., 110, D18307,

doi:10.1029/2005jd005800, 2005.
Williams J: Organic trace gases in the atmosphere, an overview, Environ. Chem., 1, 125–136, doi:10.1071/EN04057, 2004
Wittrock, F., Richter, A., Oetjen, H., Burrows, J. P., Kanakidou, M., Myriokefalitakis, S., Volkamer, R., Beirle, S., Platt, U., and Wagner, T.: Simultaneous global observations of glyoxal and formaldehyde from space, Geophys. Res. Lett., 33, L16804, doi:10.1029/2006gl026310, 2006.
Wittrock, F.: The Retrieval of oxygenated volatile organic compounds by remote sensing techniques, PhD Thesis, Bremen University, 2006.
Yu, S. C.: Role of organic acids (formic, acetic, pyruvic and oxalic) in the formation of cloud condensation nuclei (CCN): a review, Atmos. Res., 53, 185–217, 2000.
Zhou, X. L. and Mopper, K.: Apparent Partition-Coefficients of 15 Carbonyl-Compounds between Air and Seawater and between Air and Fresh-Water – Implications for Air Sea Exchange, Environ. Sci. Technol., 24, 1864–1869, 1990.
Zhou, X. L. and Mopper, K.: Photochemical production of low-molecular-weight carbonyl compounds in seawater and surface microlayer and their air-sea exchange, Marine Chem., 56, 201–213, 1997

ACPD
9, 8993–9042, 2009

Table 1. CHO.CHO concentrations in rural, semi-polluted, polluted and marine sites. The SCIAMACHY vertical columns were converted to mixing ratios using some basic assumptions noted in the caption.

Location	Comment	Period (season)	Mixing ratio (pptv)	SCIAMACHY (pptv)**	Reference
[1] Metter, Georgia, USA (32° N, 82° W)	Rural	Summer	80±60* Range: 20 – 190	316±103	Lee et al. (1995)
[2] San Nicolas, Ventura, USA (33° N, 119° W)	rural	Autumn	100	128±96	Grosjean et al. (1996)
[3] Tamakomai forest, Hokkaid, Japan (43°'N, 142° E)	Rural	Autumn	90±36* Range: 26–136	119±107	Ieda et al. (2006)
[4] Anadia, Portugal (40° N, 8° W)	Rural	Summer	Range: 0–600	89±26	Cerqueira et al. (2003)
[5] Blodgett forest, California, USA (39N, 120° W)	Rural, 1315 m	Summer	27±15, Range: 6–83	33±26	Spaulding et al. (2003)
[6] Pinnacles, Shenandoah Park, Virginia, USA (39° N, 78° W, 1037 m)	Rural (mountain site–1037 m)	Autumn	35±10* Range:10–200	93±34	Munger at el. (2005)
[7] Goldlauter, Germany, (55° N, 11° E)	Rural, 605m	Autumn	20±10* Range: 4–31	19±25	Müller et al. (2005)
[8] Lassen, California, USA (38°5'N, 121° W),	Rural, 2070 m	Summer/Autumn	Range: 0–38	106±48	Seaman et al. (2006)

* At around 10:00 a.m. as calculated from the cited diurnal variation when available

** The conversion of the column densities to pptv is performed by assuming that most of the observed CHO.CHO is found inside the boundary layer. For simplicity reasons, standard conditions for temperature (25°C) and pressure (1 atm) were used in the calculations. In addition, it was assumed that the ground based measurements are representative for the area extending by ±0.5° around them as well as for the specific season when they were contacted regardless the year of measurements (e.g. a measurement performed in August is representative for the summer).

ACPD
9, 8993–9042, 2009

Table 1. Continued.

Location	Comment	Period (season)	Mixing ratio (pptv)	SCIAMACHY (pptv)**	Reference
[9] Roseville, California, USA (38°5'N, 121° W),	Sub-urban	Summer/Autumn	143±37	118±101	Seaman et al. (2006)
[10] LA, USA, (34° N, 117° W)	Polluted/urban	Autumn	263±246 Range: 40–950	191±62	Kawamura et al. (2000)
[11a][11b] Las Vegas, USA (36° N, 115° W)	Polluted/urban	Summer Winter	Range: 120–420 Range: 90–210	78±35 51±50	Jing et al. (2001)
[12] Long Beach, LA, Claremont, Azusa, California, USA (34° N, 117° W)	Polluted/urban	Autumn	530±270* Range: 12–3800	237±94	Grosjean et al. (1996)
[13] Pabstthum, Germany (52°5'N, 12°5'E)	Polluted/urban	Summer	30±20* Range: 10–125	150±59	Moortgat et al. (2002)
[14] Mexico City, Mexico (19°3'N, 19°1'W)	Polluted/urban	Spring	200±80* Range: 0–1200	82±41	Volkamer et al. (2005)
[15] MIT, Massachusetts, USA (42°4'N, 71°1'W)	Polluted/urban	Summer	70±40* Range: 40–140	318±86	Sinreich et al. (2007)
[16] Gulf of Maine, (43°'N, 68° W)	Marine/polluted	Summer	200±150* Range: 75–350	206±79	Sinreich et al. (2007)
[17] Caribbean Sea and Sargasso Sea coast, (15° N, 66° W)	Marine	Autumn–Spring	80	89±38	Zhou and Mopper (1990)
[18] Nashville, Tennessee, USA (37° N, 87° W)	Free troposphere	Summer	67±40, range: 10–290 (inside the BL)	86±25	Lee et al. (1998)

ACPD
9, 8993–9042, 2009

Table 2. Median values of VCDs of CHO.CHO and HCHO coupled with their median ratio (R_{GF}), the average EVI and the sum of fire numbers for the period 2003–2007. Data gridded to 0.5×0.5° have been used for the analysis of the data.

	Box number/ Fig. 8	Lat center (deg)	Long center (deg)	CHO.CHO (molec cm^{-2})	HCHO (molec cm^{-2})	R_{GF}	EVI	Sum of fire counts
USA	1-a	32±4	−90±10	3.67×10^{14}	8.07×10^{15}	0.045	0.32	1061
S. America	2-b	0±10	−62±8	5.32×10^{14}	1.25×10^{16}	0.043	0.49	23 759
S. America*	3-c	−2±4	−50±3	6.62×10^{14}	1.38×10^{16}	0.048	0.47	13 198
Africa_N	4-d	6±4	1±10	5.83×10^{14}	1.14×10^{16}	0.051	0.42	11 098
Africa_Eq	5-e	2±4	19±9	5.36×10^{14}	1.29×10^{16}	0.042	0.46	3902
Africa_S	6-f	−7±5	19±9	5.05×10^{14}	1.10×10^{15}	0.046	0.39	2879
Indonesia	7-i	2±6	108±12	5.54×10^{14}	8.34×10^{15}	0.066	0.43	22 770
Australia	8-l	−14±3	135±10	3.75×10^{14}	6.09×10^{15}	0.062	0.24	21 449
Asia_S	9-k	25±3	112±5	5.79×10^{14}	1.25×10^{16}	0.046	0.35	1778
Asia_N	10-j	34±5	116±5	4.52×10^{14}	1.19×10^{16}	0.038	0.29	8057
India	11-h	24±4	85±7	4.88×10^{14}	9.14×10^{15}	0.053	0.30	2535
Europe	12-g	48±5	7±6	2.20×10^{14}	7.32×10^{15}	0.034	0.34	2127

*SA box 3 is studied due to its higher glyoxal values in comparison to box 2 (details provided at Sect. 3.5.2)

ACPD
9, 8993–9042, 2009

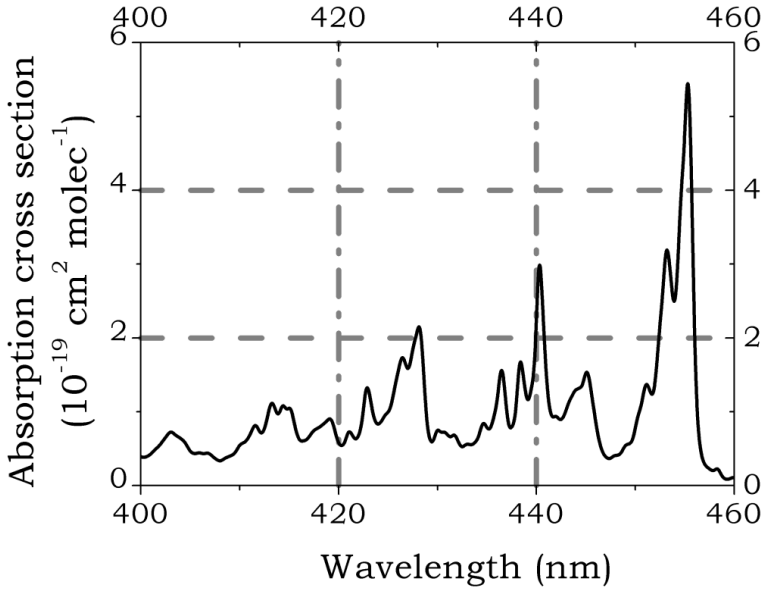

Fig. 1a. Highly resolved CHO.CHO absorption cross section (FWHM=0.001 nm) (Volkamer et al., 2005) convoluted to the SCIAMACHY slit function (FWHM=0.5). The maximum absorption cross section value of the sharp CHO.CHO peak (at 455 nm) is $\sigma_{(CHO.CHO)}=5.45\times10^{-19}$ cm^2 molec^{-1}.

ACPD
9, 8993–9042, 2009

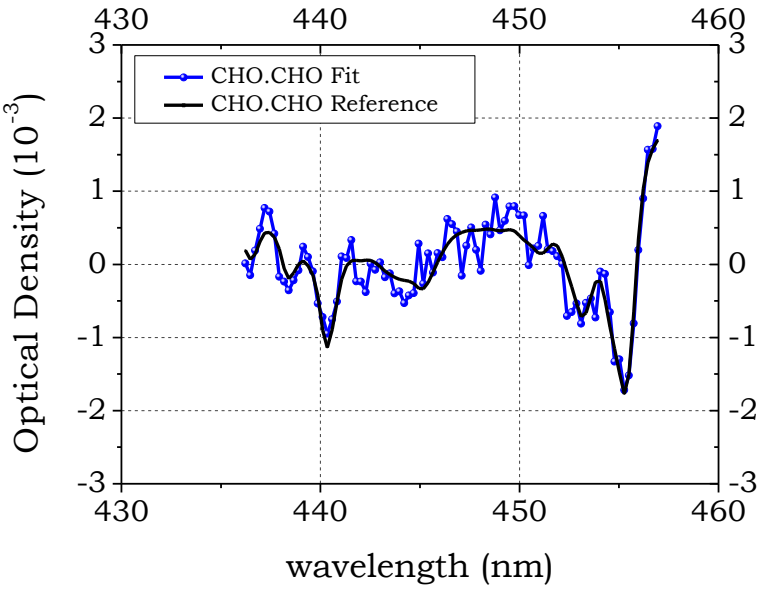

Fig. 1b. Representative example of a DOAS fit of CHO.CHO for a ground scene above a smoke plume observed during the intensive fires above Greece, on August 2007 (orbit:70826091). The blue dotted line is the CHO.CHO fitted result after removing all other absorbers and the black line depicts the scaled differential laboratory reference. The computed $SCD_{CHO.CHO}$ to this case is 6.23×10^{15} molec cm^{-2}.

ACPD
9, 8993–9042, 2009

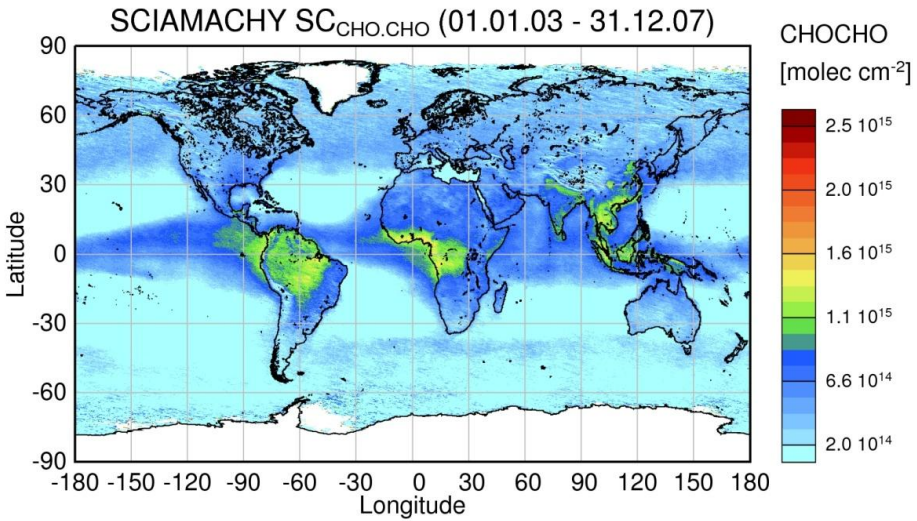

Fig. 2a. Multiannual composite map of the CHO.CHO slant column densities retrieved from the radiance measurements from the SCIAMACHY instrument.

ACPD
9, 8993–9042, 2009

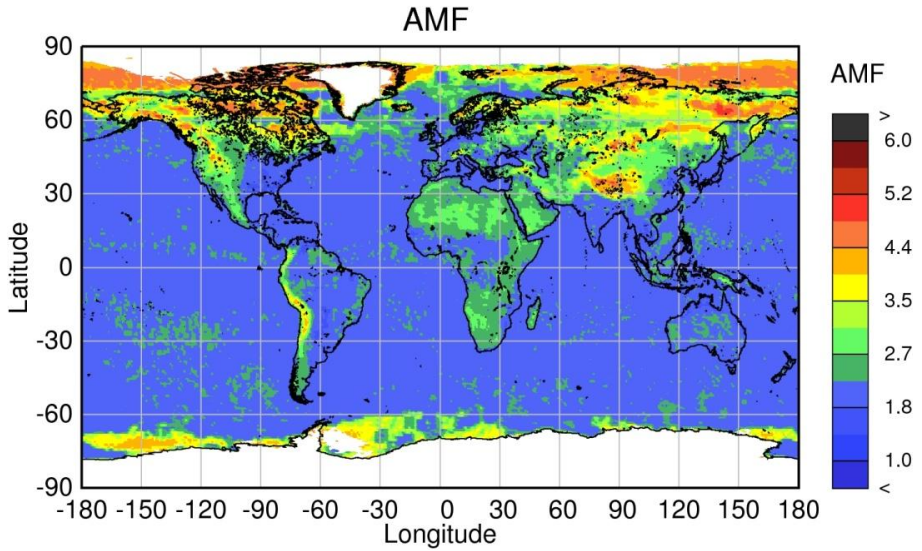

Fig. 2b. AMF: Multiannual composite map of the air mass factors computed with the radiative tranfer model SCIATRAN.

ACPD

9, 8993–9042, 2009

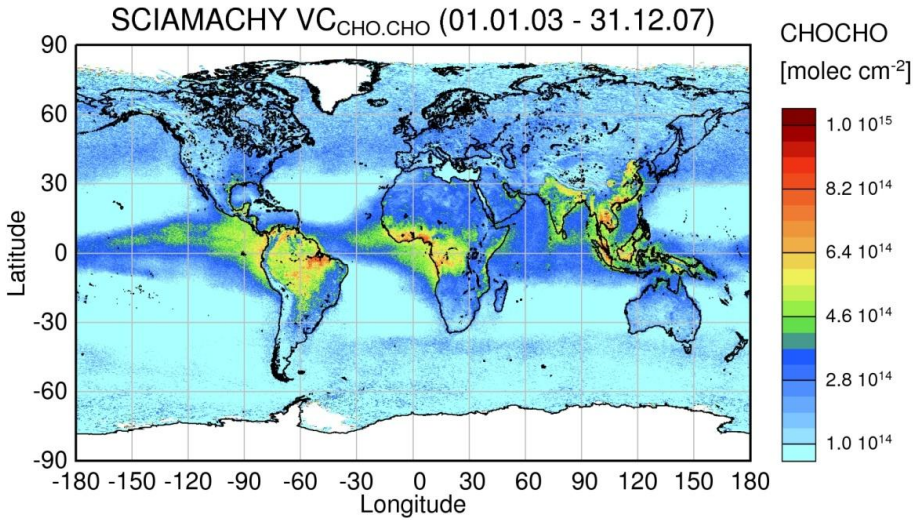

Fig. 2c. Multiannual composite map of the CHO.CHO vertical column densities computed from the ratio SCD/AMF. The largest amounts of CHO.CHO are found over the tropical and subtropical latitudes which are characterized by vegetation and fire emissions of volatile organic compounds.

ACPD
9, 8993–9042, 2009

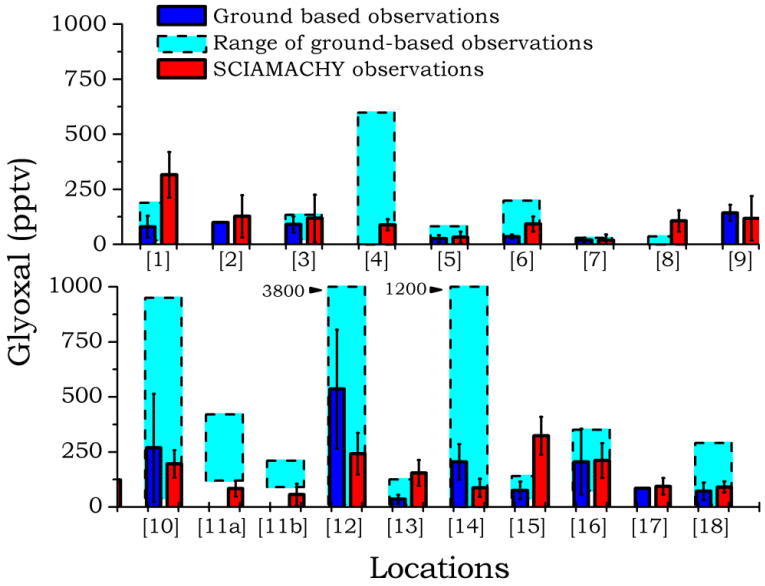

Fig. 3. Comparison of the in situ observations (blue bars) with the converted space based observations (red bars) using the assumptions stated in the text. The cyan bars depict the range of the ground based measurements. In some of the references is reported only the range and not the actual value. The numbers of the locations correspond to the measuring stations used in Table 1.

ACPD
9, 8993–9042, 2009

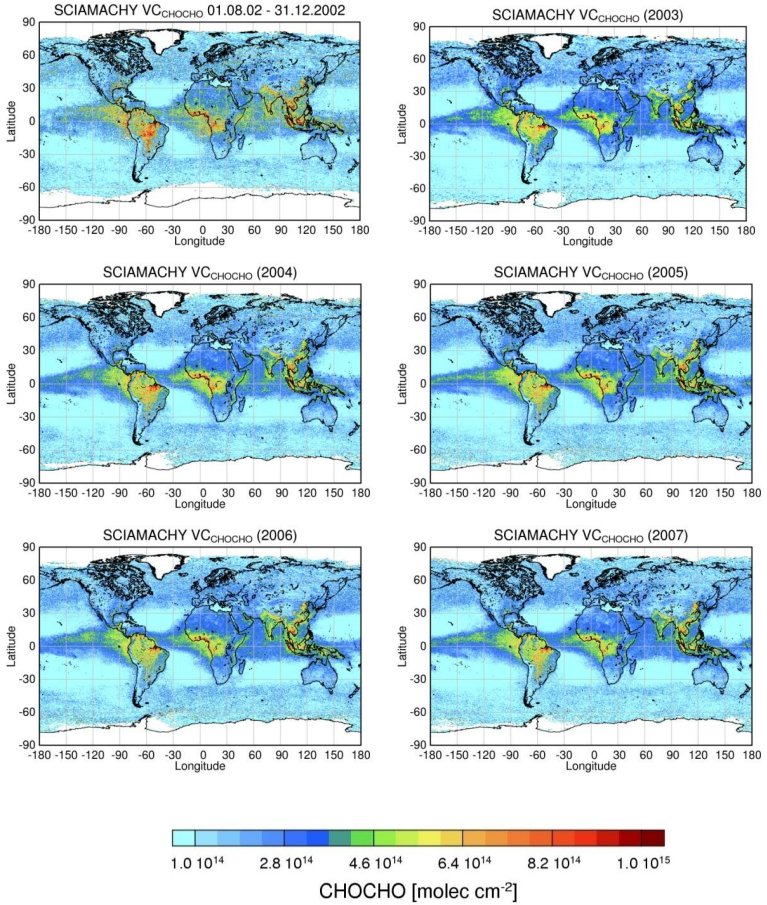

Fig. 4. $VC_{CHO.CHO}$ per year: Yearly averaged CHO.CHO vertical columns (molec cm^{-2}) from 2003 to 2007. This figure includes also the half year observations obtained during the period August 2002–December 2002.

ACPD
9, 8993–9042, 2009

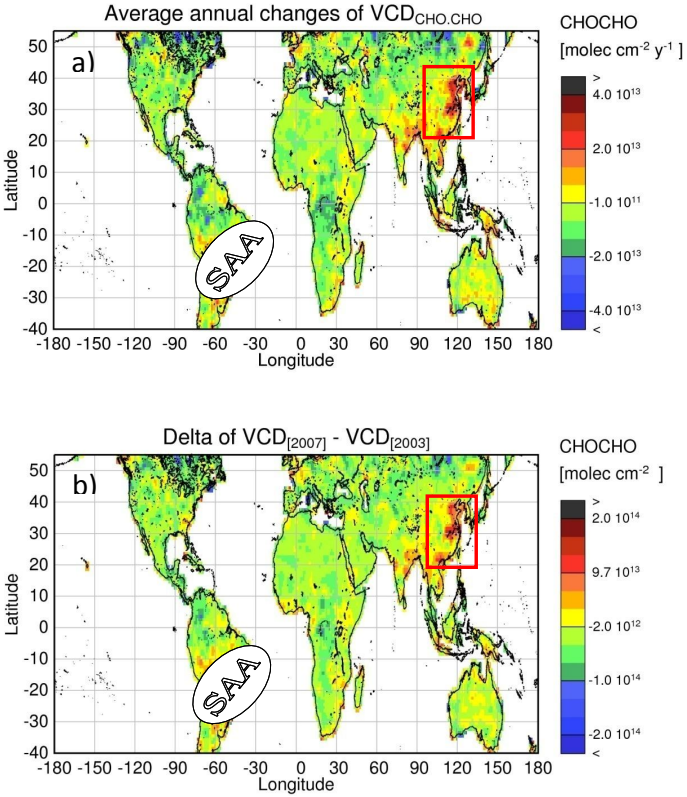

Fig. 5. Absolute and respective differences. Linear regression **(a)** of the annual averages of the CHO.CHO vertical columns retrieved for the period 2003–2007 and the difference **(b)** of the CHO.CHO vertical columns retrieved for the years 2007 and 2003. The red color denotes an increase while the blue one shows a decrease in respective $VCD_{CHO.CHO}$ values. The SAA corresponds to the South Atlantic Anomaly and the values are not considered in this study because they have more noise. Significant increases of the rate of emission of CHO.CHO is observed over China.

ACPD
9, 8993–9042, 2009

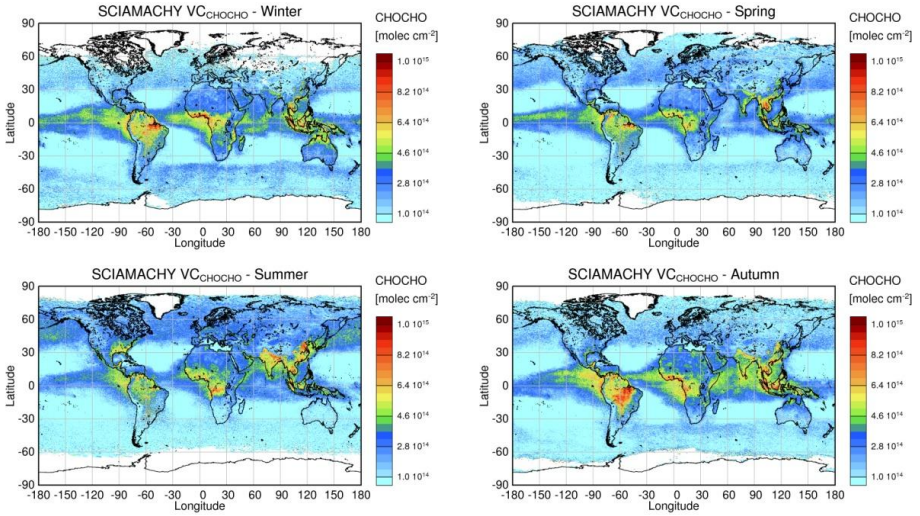

Fig. 6a. Seasonal variation of CHO.CHO: Seasonal means of CHO.CHO VCDs for December, January, and February (DJF), March, April, and May (MAM), June, July, August, (JJA) and September, October, November, (SON).

ACPD
9, 8993–9042, 2009

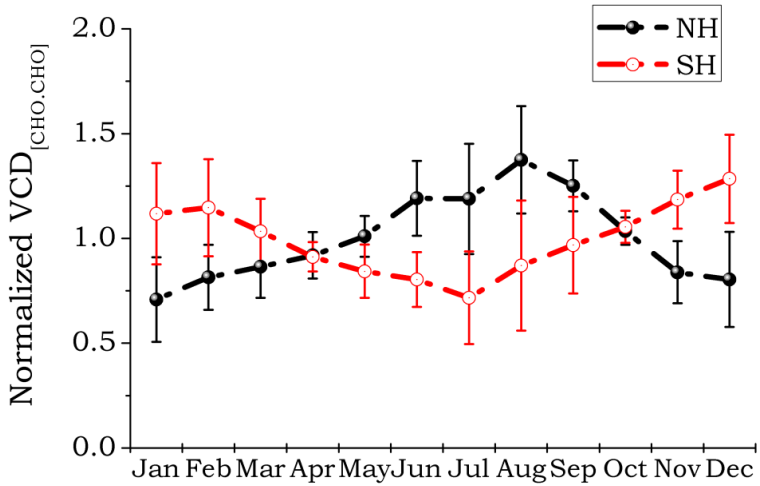

Fig. 6b. Mean normalized CHO.CHO VCDs calculated for the hot spots located in both NH (black dotted line) and SH (red dotted line) and described in Table 2.

ACPD
9, 8993–9042, 2009

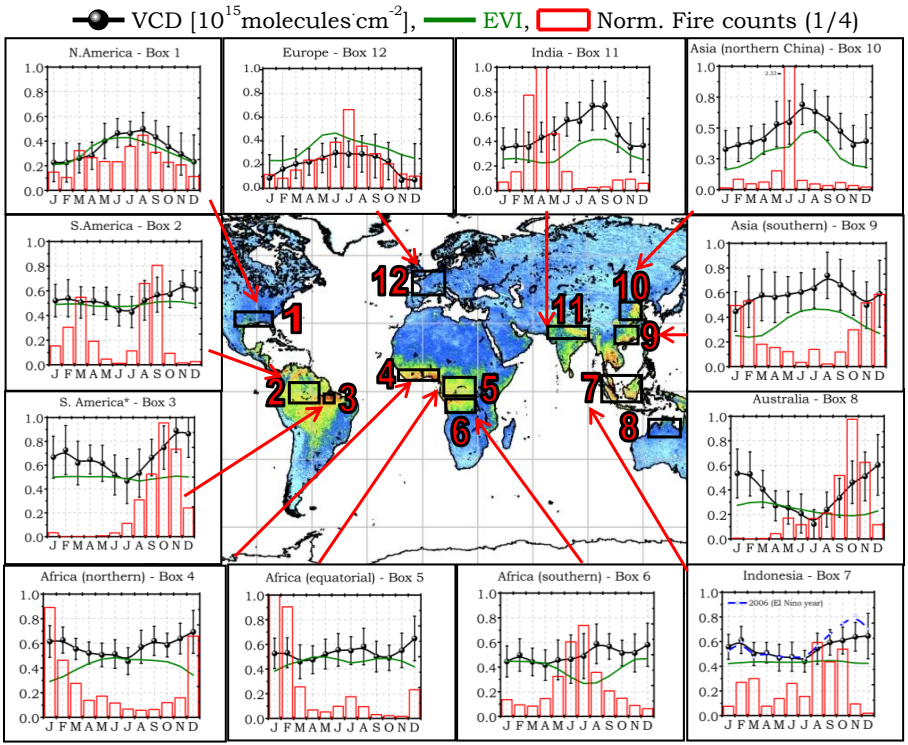

Fig. 7. Monthly mean variability of the $VCD_{CHO.CHO}$ (black dotted line) computed over the 12 selected photochemical hotspots of Table 2. The green line illustrates the Enhanced Vegetation Index calculated from MODIS data and the red columns depict the one fourth of the normalized, per year, fire counts as computed from the AATSR instrument.

ACPD
9, 8993–9042, 2009

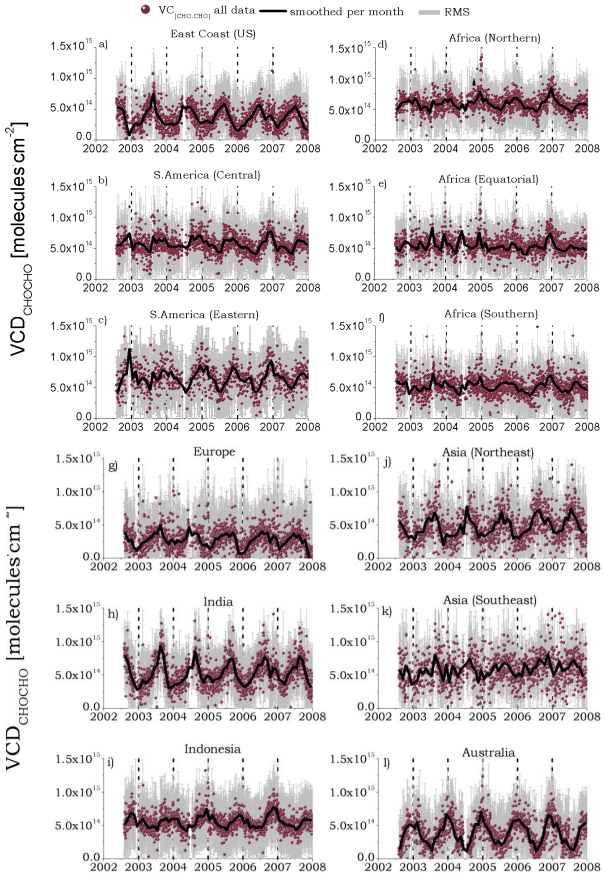

Fig. 8. Interannual variability of the vertical column densities of CHO.CHO over the selected hotspots. The dots show all the individual measurements, the black lines present the respective monthly means and the gray lines corresponds to the residual mean squares (RMS) of the fit for each individual measurement.

ACPD
9, 8993–9042, 2009

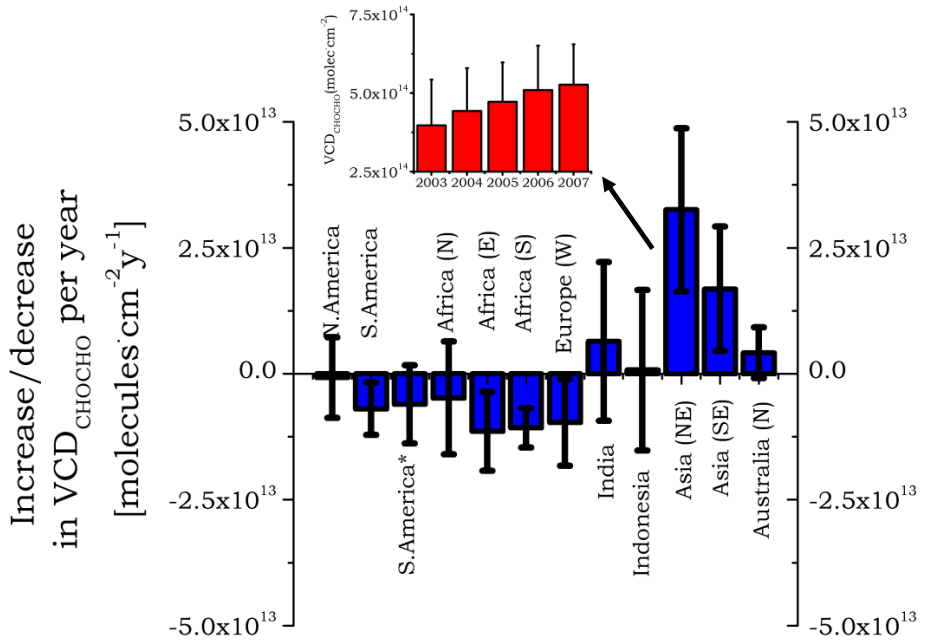

Fig. 9. Linear regression analysis of the CHO.CHO VCDs coupled with their uncertainties (2σ), over the selected hotspots of Table 2. The red columns show the annual increase of the VCDs of CHO.CHO observed over Northeastern Asia.

ACPD
9, 8993–9042, 2009